Kinetics of the Thermal Dissociation of ZnO Exposed to Concentrated Solar Irradiation Using a Solar-Driven Thermogravimeter in the 1800–2100 K Range

Lothar O. Schunk
Solar Technology Laboratory, Paul Scherrer Institute, Villigen PSI 5232, Switzerland

Aldo Steinfeld
Solar Technology Laboratory, Paul Scherrer Institute, Villigen PSI 5232, Switzerland
Dept. of Mechanical and Process Engineering, ETH Zurich, Zurich 8092, Switzerland

DOI 10.1002/aic.11765
Published online April 27, 2009 in Wiley InterScience (www.interscience.wiley.com).

The two-step H_2O-splitting thermochemical cycle based on the Zn/ZnO redox reactions is considered for solar H_2 production, comprising the endothermal dissociation of ZnO followed by the exothermal hydrolysis of Zn. A solar-driven thermogravimeter, in which a packed-bed of ZnO particles is directly exposed to concentrated solar radiation at a peak solar concentration ratio of 2400 suns while its weight loss is continuously monitored, was applied to measure the thermal dissociation rate in a set-up closely approximating the heat and mass transfer characteristics of solar reactors. Isothermal thermogravimetric runs were performed in the range 1834–2109 K and fitted to a zero-order Arrhenius rate law with apparent activation energy 361 ± 53 kJ mol^{-1} K^{-1} and frequency factor $14.03 \times 10^6 \pm 2.73 \times 10^6$ kg m^{-2} s^{-1}. Application of L'vov's kinetic expression for solid decomposition along with a convective mass transport correlation yielded kinetic parameters in close agreement with those derived from experimental data. © 2009 American Institute of Chemical Engineers *AIChE J*, 55: 1497–1504, 2009

Keywords: zinc, zinc oxide, decomposition, dissociation, kinetics, thermogravimeter, thermochemical cycle, hydrogen, solar, energy, radiation, ablation

Introduction

Solar thermochemical processes for hydrogen production make use of concentrated solar radiation as the energy source of high-temperature process heat.[1] Several 2-step H_2O-splitting thermochemical cycles based on metal oxides redox reactions are being considered.[2–5] Of special interest is the one based on the ZnO/Zn redox pair, comprising: (1) the solar endothermal dissociation of ZnO(s) into its elements; and (2) the nonsolar exothermal steam-hydrolysis of Zn into H_2 and ZnO(s), and represented by

$$\text{First step (solar ZnO-decomposition):} \quad ZnO \rightarrow Zn + 0.5O_2 \tag{1}$$

$$\text{Second step (nonsolar Zn-hydrolysis):} \quad Zn + H_2O \rightarrow ZnO + H_2 \tag{2}$$

H_2 and O_2 are derived in different steps, thereby eliminating the need for high-temperature gas separation. This cycle has

Correspondence concerning this article should be addressed to A. Steinfeld at aldo.steinfeld@eth.ch.

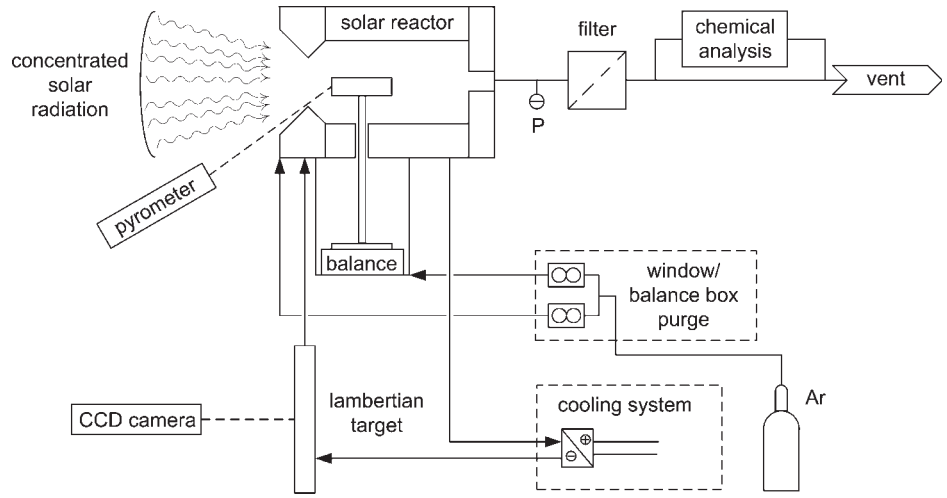

Figure 1. Solar TG experimental set-up at the solar furnace.

The ZnO sample is directly exposed to concentrated solar radiation, while its weight loss during the thermal decomposition is continuously monitored.

been identified as a promising path for solar H_2 production from H_2O because of its potential of reaching high energy conversion efficiencies and consequently economic competitiveness.[6,7] Assuming a solar reactor operating at 2000 K, subjected to a solar concentration ratio of 5000 suns* and with 50% sensible/latent heat recovery, the theoretical solar-to-chemical energy conversion efficiency can exceed 40%. A life cycle assessment indicates a 90% reduction of greenhouse gas emissions derived from fuel cell cars driven by solar hydrogen compared to those derived from advanced fossil fuel powertrains.[8] The second step of the cycle, Eq. 2, has been experimentally demonstrated using an aerosol-flow reactor that features in situ formation and hydrolysis of Zn nanoparticles.[9] The focus of this study is to establish the kinetics of the first step of the cycle when ZnO is directly exposed to concentrated solar radiation.

Several chemical aspects of the thermal dissociation of ZnO, Eq. 1, have been previously investigated.[10] At 2340 K, $\Delta G^\circ = 0$ kJ mol^{-1} and $\Delta H^\circ = 395$ kJ mol^{-1}. ZnO decomposes into its constituents rather than subliming into ZnO(g).[11–14] Values of the apparent activation energy determined by thermogravimetry in vacuum ranged from 311 to 327 kJ mol^{-1} for sintered ZnO tubes, 50–100 μm layers, and single-crystals at 1136 to 1385°K,[12] 356 kJ mol^{-1} for ZnO spinel at 1608 to 1773 K,[15] and 373 $\pm$ 6 kJ mol^{-1} for ZnO particles at 1255 to 1258 K.[16] Reported values for the activation energy of dissociation in a buffer gas atmosphere were 312–376 kJ mol^{-1} for ZnO particles (1 μm mean particle size) in N_2 at 1273 to 1823 K,[17] 353 $\pm$ 26 kJ mol^{-1} for ZnO particles (50 nm and 1 μm) in Ar at 1713 to 2023 K,[18] and 329 kJ mol^{-1} for directly irradiated presintered ZnO pellets.[19] Nonstoichiometry and lattice defects were found to affect the kinetics under vacuum at 1013 and 1053 K.[13] Exploratory tests were carried out in solar furnaces with batch reactors.[20–23] Recently, a 10 kW solar chemical reactor prototype featuring a rotating cavity-receiver lined with ZnO particles has been experimentally demonstrated in a solar furnace.[24] This reactor uses a multilayer cylindrical cavity-receiver made of sintered ZnO tiles placed on top of a porous 80% Al_2O_3–20% SiO_2 insulation and reinforced by a 95% Al_2O_3–5% Y_2O_3 ceramic matrix composite, providing mechanical, chemical, and thermal stability and a diffusion barrier for product gases. An important property of this reactor concept is that the ZnO particles are directly exposed to concentrated solar radiation and serve the functions of radiant absorbers, thermal insulators, and chemical reactants. The accurate determination of the reaction kinetics of particulate ZnO under extreme solar reactor conditions (temperatures $>$ 2000 K and heating rates $>$ 100 K/s) required the development of a novel solar-driven thermogravimeter that approaches the heat and mass transfer characteristics existing in the solar reactor and enables on-line monitoring of the weight loss as a function of time and temperature. This paper describes the design and fabrication of this unique apparatus and presents its application for measuring the ZnO dissociation rate at up to 2100 K in a solar furnace.

The solar thermogravimeter (TG)

The solar thermogravimeter (solar TG) is shown schematically in Figure 1. It consists of a solar cavity-receiver, i.e. a well-insulated cylindrical enclosure of i.d. 152 mm and length 150 mm, lined with 50 mm-thick CaO-stabilized ZrO_2 bricks over two layers of 36 mm-thick porous Al_2O_3. It has a 60 mm-diameter circular opening—the aperture—for the access of concentrated solar energy through a transparent 3 mm-thick quartz window. Inside the cavity, the ZnO sample is mounted on an Al_2O_3 rod that is suspended on a balance (Mettler Toledo; accuracy 0.01 g). With this arrangement, the ZnO sample is directly exposed to concentrated solar radiation, while its weight loss during decomposition is continuously monitored on-line.

An Ar flow, injected tangentially and radially at the aperture plane, creates an aerodynamic curtain that protects the window from condensable products and carries the gaseous products Zn(g) and O_2 to the outlet port at the rear of the

*The solar flux concentration ratio C is defined as the solar radiative flux achieved after concentration, normalized to 1 sun = 1 kW/m^2.

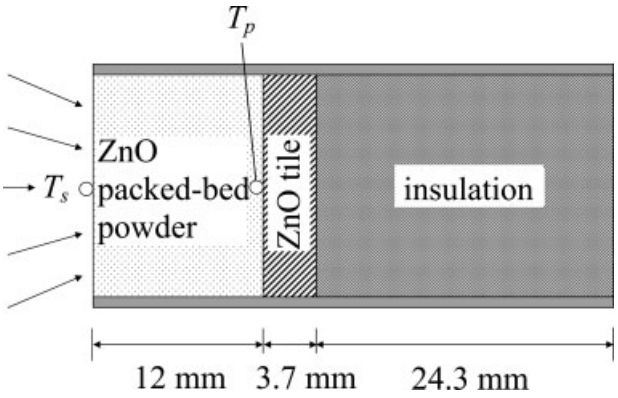

Figure 2. Schematic of sample used in the solar TG.

Indicated is the location of the temperature measurements: T_p of the ZnO tile is measured by a type-B thermocouple, and T_s of the irradiated front surface of the ZnO packed-bed powder is measured by a solar-blind pyrometer.

cavity. Ar gas is also introduced into the box containing the balance to prevent back-flow of hot gases. Downstream, the Zn(g) is condensed and filtered (glass microfibre filter with pore size of 2.7 μm), and the gas composition is analyzed. Experimentation was carried out at PSI's solar furnace[25]: a sun-tracking flat heliostat on-axis with a stationary primary paraboloidal concentrator. Peak solar flux concentration ratios exceeding 5000 suns can be achieved at the focal plane, enabling the sample in the solar TG to attain stagnation temperatures[†] above 2500 K at ultra-high heating rates faster than 1000 K/s. Solar flux intensities, regulated with a Venetian-type shutter located between the heliostat and the solar concentrator, are measured optically with a calibrated CCD camera on a water-cooled Al_2O_3-plasma coated Lambertian target. The camera also allows for sample visualization during the experimental runs. Sample surface temperatures are measured with a solar-blind pyrometer that is not affected by the reflected solar irradiation because it measures in a narrow wavelength interval around 1.39 μm where solar irradiation is mostly absorbed by the atmosphere.[26] The composition of the product gases is monitored by gas chromatography (Agilent High Speed Micro GC G2890A, equipped with molecular sieve 5A and HaySep A capillary columns, detection limit = 10 ppm; sampling rate = 0.33 min^{-1}), by IR-based detectors for CO and CO_2 (Siemens Ultramat 23, detection limits = 0.2%; sampling rate = 1 s^{-1}), and by thermal conductivity-based detectors for H_2 and O_2 (Siemens Calomat 6 and Oxymat 6, accuracy = 50 ppm, sampling rate = 1 s^{-1}). The measurement of CO and CO_2 is carried out to verify that no carbothermic reduction occurs. Particle size distribution is measured by laser scattering (HORIBA LA-950 analyzer). BET specific surface area (SSA) is measured by N_2 adsorption at 77 K (Micromeritics 3000).

The sample investigated is depicted in Figure 2. It consists of 20 mm-i.d. 40 mm-length Al_2O_3 tube containing the same multilayer arrangement of the solar reactor[24]: a 12 mm-thick packed-bed of ZnO powder (Alpha Aesar No. 11558, mean particle size = 0.96 μm, SSA = 6.23 m^2 g^{-1}), followed by a 3.7 mm-thick sintered ZnO tile and a 24 mm-thick 80% Al_2O_3–20% SiO_2 porous insulation. The total mass of ZnO powder was 6.2 g, with an average porosity of 70.3% $\pm$ 0.4%. The temperature of the ZnO tile, T_p, is measured with a type-B thermocouple. The temperature of the irradiated front surface of the ZnO packed-bed powder, T_s, is measured with the solar-blind pyrometer.

Experimental Procedures

The cavity was first purged with Ar gas until the O_2 concentration was less than 100 ppm. With this residual O_2, the dissociation of ZnO in Ar at 1 bar total pressure is thermodynamically favorable at above 1470 K, according to the equilibrium composition calculated with the HSC code.[27] The Ar flow was maintained at 12 l_N min^{-1} at the aperture and at 3 l_N min^{-1} at the balance box.[‡] During a typical solar experimental run, the solar furnace's shutter was opened to achieve the desired solar flux intensity, while the irradiated front surface of ZnO packed-bed powder was heated to the desired temperature in less than 50 s and maintained isothermally during dissociation for at least 150 s. The front surface of the ZnO packed-bed powder was exposed to a peak and a mean solar flux concentration ratio of 2400 and 2200 suns, respectively. The duration of a single run never exceeded 720 s to avoid variations of the solar irradiation or condensation of products on the quartz window, which affect the desired isothermal conditions. No CO and CO_2 were detected during all runs, ensuring that ZnO was not reduced carbothermally. Zn reoxidation occurred downstream but no effort was undertaken to quench the products and avoid their recombination. Figure 3 shows SEMs of (a) initial ZnO powder sample; and (b) recombined gaseous products collected in the filter, downstream of the solar TG. The ZnO reacting particles exhibited a wurtzite-type crystal structure with no visible microporosity, indicating that their average porosity was due mainly to interparticle void space. The product particles collected in the filter exhibit a tetrapod-like structure formed by growth of ZnO crystal with wurtzite structure as a result of nucleation, condensation, and reoxidation of Zn(g) under supersaturation.[28–30]

Results and Discussion

Seven isothermal solar experimental runs, performed in the range 1834–2109 K, are summarized in Table 1. Listed are the mean effective surface temperature T_s, the mass loss of the ZnO batch Δm during the period of evaluation of length Δt, associated mass loss rate dm/dt per unit of effective (irradiated) surface area, total fractional conversion α_{max}, and normalized linear regression coefficient of the fitted mass loss curve. The ZnO packed-bed's front surface temperature T_s was determined from the measured pyrometer temperature $T_{pyrometer}$ byT1

$$T_s = (\tau_w \varepsilon_{ZnO})^{0.25} T_{pyrometer} \quad (3)$$

where τ_w is the window transmissivity and ε_{ZnO} is the emissivity of ZnO at the pyrometer's operational wavelength,

†The stagnation temperature is the highest temperature an ideal blackbody solar cavity-receiver is capable of achieving when solar energy is being reradiated as fast as it is absorbed. It is given by $(IC/\sigma)^{0.25}$, where I is normal beam insolation, C is the solar flux concentration ratio, and σ is the Stefan-Boltzmann constant.

‡l_N means liters at normal conditions; mass flow rates are calculated at 273 K and 1 bar.

Table 1. Summary of the Solar Experimental Runs: Mean Effective Surface Temperature T_s, Mass Loss of the ZnO Batch Δm During the Period of Evaluation of Length Δt, Associated Mass Loss Rate dm/dt Per Unit of Effective Surface Area, Total Fractional Conversion α_{max}, and Normalized Linear Regression Coefficient of the Fitted Mass Loss curve

run #	T_s (K)	Δm (mg)	Δt (s)	dm/dt (kg^{-2} m^{-2} s^{-1})	α_{max} (-)	R^2
1	2109.1	380	140	0.0176	0.125	0.997
2	1977.8	90	170	0.0034	0.024	0.968
3	1889.8	80	250	0.0021	0.016	0.982
4	1902.1	70	250	0.0018	0.027	0.977
5	1833.6	30	300	0.0006	0.010	0.832
6	2038.6	330	300	0.0071	0.061	0.998
7	1945.6	110	280	0.0025	0.021	0.988

1.39 μm. $\tau_w \varepsilon_{ZnO} = 0.69$ was determined using flash-assisted multiwavelength pyrometry.[31,32] Surface temperature fluctuations of about ± 10 K were observed in several runs and ascribed to fluctuations in the solar irradiation.

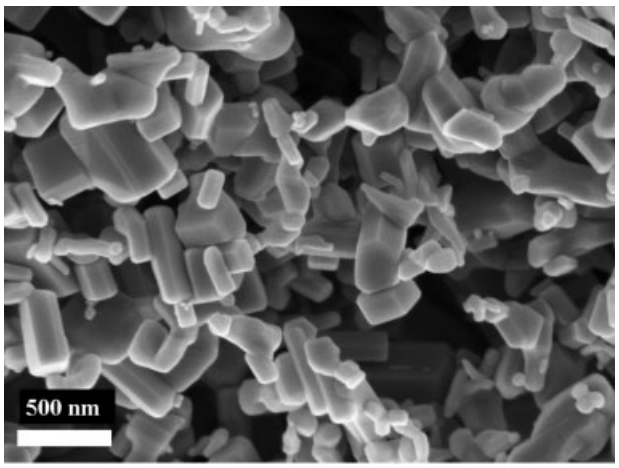

(a)

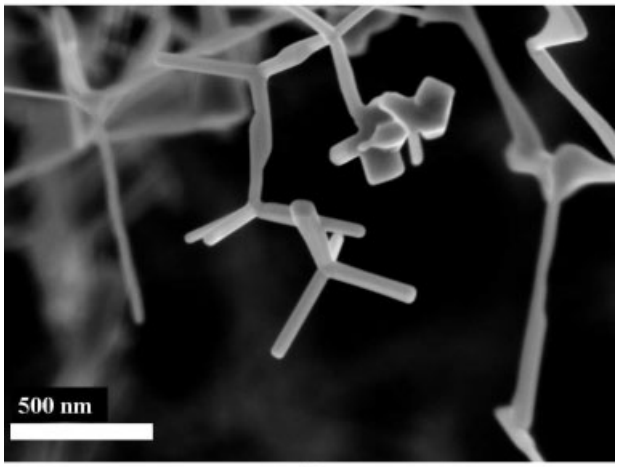

(b)

Figure 3. SEM of (a) initial ZnO powder placed in the solar TG; and (b) recombined gaseous products collected in the filter.

The packed-bed sample of ZnO powder underwent up to 50% shrinkage during the initial 30 s due to sintering, as observed with the CCD camera. This resulted in an overall porosity change from 70% to up to 40% before the onset of decomposition, creating a thin and dense topmost layer. The initial relative weight loss was less than 1% and may be attributed to nonstoichiometry, contraction, and lattice defects.[13] Δm was evaluated after 75 s to bypass initiation effects by sintering and to ensure negligible surface area change and stationary surface temperature T_s. Δm resulted from the weight loss of the batch of ZnO packed-bed powder exclusively; no reaction between ZnO and Al_2O_3 was detected. Furthermore, the ZnO tile did not contribute to Δm since its measured temperature T_p was at least 250 K lower than T_s, and its surface showed no sign of dissociation after each experimental run.

The ZnO packed-bed surface temperature and sample weight loss as a function of time are shown in Figure 4 during a representative solar TG run (No. 6). The ZnO packed-bed surface was heated to 1300 K at a rate of 150 K/s once exposed to a mean solar concentration of 1400 suns, and further heated to 2038 K at a rate of 20 K/s. Color change from white to black was recorded by the CCD camera due presumably to nonstoichiometry at the surface[33] (formed by either preferential removal of O from the surface[12,34] or outward diffusion of interstitial Zn[35]), which in turn resulted in a dramatic increase of the total effective absorptivity from 0.05 to 0.15 at room temperature[36] to about 0.9 at 2000 K.[19] Measurable weight loss was detected at above about 1825 K ($t = 30$ s) and continued at a constant rate until the shutter was closed and the run terminated. The packed bed of ZnO powder was subjected to a transient ablation regime, characterized by a rate of heat transfer—predominantly by radiation—to the top layer of the packed bed undergoing endothermic dissociation that proceeded faster than the rate of heat transfer—predominantly by conduction—to the depth of the packed bed.

T_s and dm/dt listed in Table 1 were used in the Arrhenius plot of Figure 5. Applying a zero-order rate equation for linear advance of the interface in a single direction,[37] the rate

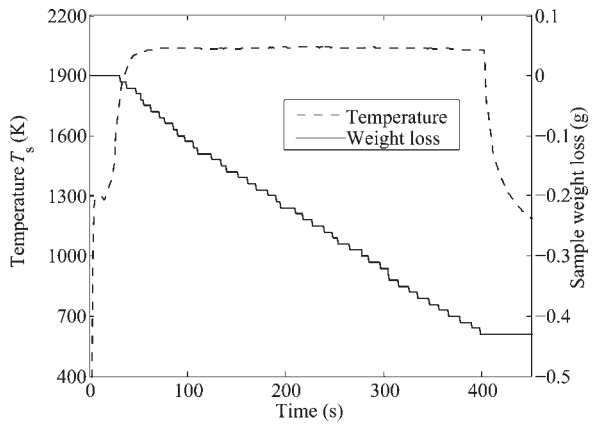

Figure 4. Irradiated surface temperature and weight loss of the ZnO packed-bed powder as a function of time during a representative solar TG run (No. 6).

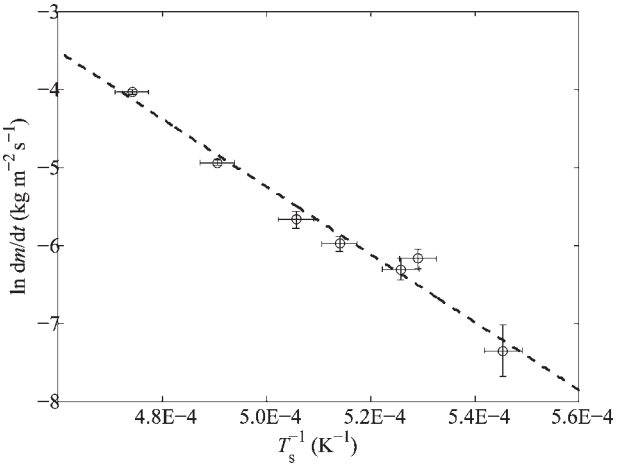

Figure 5. Arrhenius plot for the rate law, Eq. 4.

The dissociation rate is given per unit effective surface area.

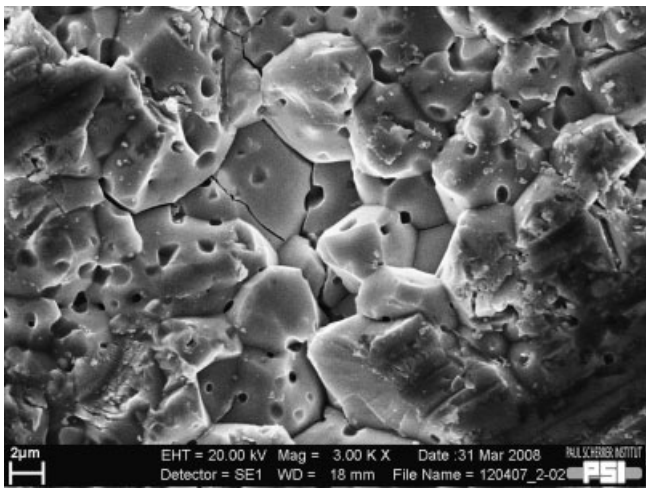

Figure 6. SEM of cross section of a ZnO sample taken 3 mm behind the irradiated surface that underwent sintering and dissociation at T_s = 1960 K for 290 s.

law is given in terms of the mass loss per unit of effective (irradiated) surface area as:

$$\frac{dm}{dt} = Ak_0 e^{E_a/RT_s} \tag{4}$$

The corresponding apparent activation energy $E_a = 361 \pm 53$ kJ mol^{-1} K^{-1} and frequency factor $k_0 = 14.03 \times 10^6 \pm 2.73 \times 10^6$ kg m^{-2} s^{-1}, each at 95% confidence, were extracted by linear regression. The uncertainty bounds are mainly due to the emissivity value and the balance resolution. Note that, in contrast to conventional thermogravimetric runs, only the irradiated front surface shrinks in the solar TG, as a result of the ablative heat transfer characteristics in which the sample is subjected. A shrinking core model was not able to describe the reaction rate properly. Instead, an effective surface area A—the actual area of the ZnO sample that is exposed to the concentrated solar irradiation—was introduced in Eq. 4. For the dm/dt values calculated in Table 1, A was a circle of diameter $d = 14.0 \pm 0.5$ mm (determined after sintering), as the CCD camera showed that A did not change during the thermal dissociation. The sample's density, measured by pyknometer after the run, was 5.6 ± 0.056 g cm^{-3}.

Previous studies have identified surface diffusion as the rate-controlling step during the early stages of sintering with activation energies in the range 12.5–106 kJ mol^{-1}, and lattice diffusion during the intermediate and final stages of sintering at above the Tammann temperature (~1124 K), with activation energies in the range 223–276 kJ mol^{-1}.[38–40] For all runs listed in Table 1, the high heating rates achieved with concentrated solar radiation resulted in rapid sintering of the ZnO sample before any dissociation recorded by the weight loss, as expected from the higher activation energy of dissociation as compared to that of sintering. A SEM of a cross section, 3 mm behind the irradiated surface of a ZnO sample that underwent sintering and dissociation at T_s = 1960 K for 290 s is shown in Figure 6. The temperature difference $T_s - T_p$ across the sample exceeded 300 K. Noninterconnected pores of 0.3–0.8 μm diameter are predominantly located at the grain boundaries, as previously observed during final stages of sintering at about 1650 K.[40] The dissociation of ZnO occurred mainly at the external surface exposed to concentrated solar radiation, supporting the ablation regime. Note that thermal dissociation reactions conducted under concentrated solar energy at 2000 K and above have been shown to be primarily limited by the rate at which the gaseous products diffuse from sample surface.[14,41–43] The diffusion of gaseous products from the ZnO surface into the surrounding gas was found to be rate-controlling mechanism also at lower temperatures (1013 K).[13] Thus, k_0 may strongly depend on the purge gas conditions, and can be appropriately determined as a function of the purge gas flow rate by applying L'vov theory,[44] shown in the next section. In the range 1800–2100 K, the equilibrium pressure of the product gases varies by more than one order of magnitude, while k_0 varies

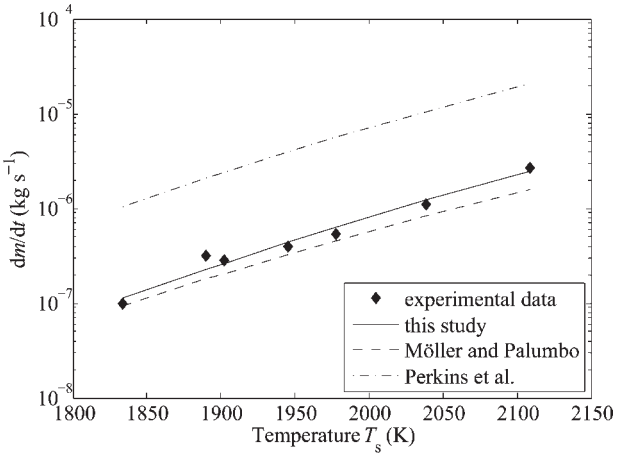

Figure 7. ZnO dissociation rate vs. temperature for the rate law derived in the present study Eq. 4, and for those derived by Möller and Palumbo[19] and by Perkins et al.[18]

The data points correspond to the values obtained experimentally.

by only 13% in that range and is practically insensitive to the change in the thermodynamic equilibrium conditions.

The value of E_a is in good agreement with those found previously.[11,17–19] Figure 7 shows the rate of ZnO dissociation as a function of temperature, in terms of mass loss per unit time of the experimental data listed in Table 1 (data points), and by applying the rate law, Eq. 4, derived in the present study (solid curve). Also included are the ZnO dissociation rates calculated using the rate laws derived by Möller and Palumbo[19] and by Perkins et al.[18] Note that the former authors applied a zero-order kinetic model to presintered ZnO pellets, while the latter authors applied a shrinking core model to particulate ZnO,

$$\frac{d\alpha}{dt} = k^* e^{\frac{-E_a}{R}\left(\frac{1}{T}-\frac{1}{T_0}\right)} (1-\alpha)^{2/3} \tag{5}$$

with $T_0 = 1895$ K, $E_a = 353 \pm 25.9$ kJ/mol, and $k^* = 3.58 \times 10^{-4} \pm 6.30 \times 10^{-5}$ s^{-1} determined by conventional (nonsolar) thermogravimetry, i.e. without direct solar irradiation. Reasonable good agreement is found between the curve of this study, obtained by on-line measurements, and that predicted by Möller and Palumbo,[19] calculated from the weight loss measured after the reaction. In contrast, Perkins et al.[18] predict a reaction rate that is about one order of magnitude higher because of the fundamental differences in heat and mass transfer mechanisms and surface area per unit mass between their experimental setup (extrapolated to an aerosol flow reactor) and the ZnO packed bed of the present study. Exposing the sample to high-flux solar irradiation provides an efficient means of radiative heat transfer directly to the reaction site. The UV portion of the incident radiation may photochemical enhance the reaction kinetics.[45] However, the high heating rates applied to the packed bed significantly alter the reacting surface by sintering. Similar ZnO sintering was observed with microwave heating at densification rates which are up to four times faster compared to low heating rates typical for laboratory thermogravimetric runs.[46,47]

It is possible to estimate the frequency factor from the thermodynamic properties of the materials and from the convective flow conditions by applying L'vov's kinetic expressions[44] based on the Hertz-Knudsen-Langmuir theory for a condensing substance in an inert gas environment and in thermodynamic equilibrium. The following expressions for the Arrhenius kinetic parameters are employed:

$$E_a = \frac{\Delta H^\circ_T}{a+b} \qquad \text{in J mol}^{-1} \tag{6}$$

$$k_0 = \frac{M_M D_M^{\frac{a}{a+b}} D_O^{\frac{b}{a+b}}}{z\,RT} \left(\frac{a}{a^{\frac{a}{a+b}} b^{\frac{b}{a+b}}}\right) e^{\frac{\Delta S^\circ_T}{R(a+b)}} \quad \text{in kg m}^{-2}\text{s}^{-1} \tag{7}$$

where D is the binary diffusion coefficient of oxygen (O) or metal (M) in the buffer gas, M_M the molecular mass of the solid, a and b are the stoichiometric coefficients of metal and oxygen in the starting oxide, respectively, T is the temperature of decomposition, ΔH°_T and ΔS°_T are the standard entropy and enthalpy of reaction, respectively, and R is the ideal gas constant. z is the diffusion distance to the buffer gas location where the concentration of the substance drops to zero. For ZnO decomposition in an Ar buffer gas atmosphere, the convective mass transport coefficient is introduced,[48] $k = D/Z$, and calculated using a correlation for a flow normal to a disk[49]:

$$Sh = \frac{kd}{D} = \frac{8}{\sqrt{2\pi}} \left(\frac{d_S}{d}\right)^{1/2} \left(\frac{\text{Re}Sc}{4n} - \frac{d}{d_S}\right)^{1/2} \quad \text{with } n = \frac{L}{d_S} \tag{8}$$

where the Sherwood (Sh), Reynolds (Re), Schmidt (Sc) numbers are based on the disk diameter d, the jet tube diameter d_S (flow source), and the distance between the disk and the jet tube L. At 2000 K and for $L = 0.05$ m, $d_S = 0.06$ m (aperture diameter), $d = 0.0072$ m, $Re = 22.1$, $D_{Zn\text{-}Ar} = 535.7 \cdot 10^{-6}$ m^2 s^{-1}. (L'vov[50]), and $Sc = 0.63$, Eq. 8 yields $Sh = 18.56$, $k = 0.70$, and $z = 771 \times 10^{-6}$ m. Further applying Eq. 7 for $D_{O\text{-}Ar} = 962.4 \times 10^{-6}$ m^2 s^{-1} (Fuller[51]), $\Delta H^\circ_T = 712.3$ kJ mol^{-1}, and $\Delta S^\circ_T = 272.4$ J mol^{-1} K^{-1} at 2000 K, it yields $k_0 = 5.99 \times 10^6$ kg m^{-2} s^{-1}, which is of the same order of magnitude as the experimentally determined value. Discrepancies between calculated and experimentally determined k_0 may be attributed to turbulences in the Ar flow from its injection position at the quartz window across the aperture to the ZnO sample surface, and buoyancy effects at the hot ZnO sample surface. Eqs. 7 and 8 may be used to evaluate k_0 at buffer gas flow conditions different to those observed in the present study. Since Sh scales with the square root of the flow velocity, the reaction kinetics can be enhanced by increasing the flow velocity across the ZnO surface. Using Eq. 6, $E_a = 356$ kJ mol^{-1}, which compares well with the value experimentally determined.

Operating conditions in the solar TG were typical of an ablation regime controlled by the rate of radiative heat transfer to the first layers of ZnO undergoing endothermic dissociation.[52] The ZnO dissociation reaction occurred in the topmost layers at the highest temperatures, as radiative transfer to the exposed (effective) surface A proceeded at a faster rate than heat conduction across the packed-bed.

Summary and Conclusions

We have carried out an experimental investigation using a novel solar-driven thermogravimeter for the determination of the ZnO dissociation kinetics under direct high-flux solar irradiation in a solar furnace. Experimental data was fitted to a zero-order Arrhenius rate law, yielding an apparent activation energy that is in close agreement with the theoretical value obtained by applying L'vov's kinetic expressions along with a correlation for convective mass transport across the ZnO packed-bed surface. Sintering was observed before ZnO dissociation. The packed bed of ZnO powder was subjected to an ablation regime characterized by a rate of radiative heat transfer to the top layer of ZnO packed bed undergoing endothermic dissociation that proceeded faster than the rate of conductive heat transfer to the depth of the packed bed.

Acknowledgements

Financial support by the Swiss Federal Office of Energy (SFOE) is gratefully acknowledged. The authors thank N. Rotering, S. Wepf, D. Wuillemin, and A. Meier for technical support during the experimental campaign at PSI's solar furnace.

Literature Cited

1. Steinfeld A. Solar thermochemical production of hydrogen–a review. *Solar Energy*. 2005;78:603–615.
2. Abanades S, Flamant G. Thermochemical hydrogen production from a two-step solar-driven water-splitting cycle based on cerium oxides. *Solar Energy*. 2006;80:1611–1623.
3. Agrafiotis C, Roeb M, Konstandopoulos AG, Nalbandian L, Zaspalis VT, Sattler C, Stobbe P, Steele AM. Solar water splitting for hydrogen production with monolithic reactors. *Solar Energy*. 2005; 79:409–421.
4. Inoue M, Hasegawa N, Uehara R, Gokon N, Kaneko H, Tamaura Y. Solar hydrogen generation with $H_2O/ZnO/MnFe_2O_4$ system. *Solar Energy*. 2004;76:309–315.
5. Kodama T, Nakamuro Y, Mizuno T. A two-step thermochemical water splitting by iron-oxide on stabilized zirconia. *J Solar Energy Eng*. 2006;128:3–7.
6. Haueter P, Moeller S, Palumbo R, Steinfeld A. The production of zinc by thermal dissociation of zinc oxide–solar chemical reactor design. *Solar Energy*. 1999;67:161–167.
7. Perkins C, Weimer AW. Likely near-term solar-thermal water splitting technologies. *Int J Hydrogen Energy*. 2004;29:1587–1599.
8. Felder R, Meier A. Well-to-wheel analysis of solar hydrogen production and utilization for passenger car transportation. *J Solar Energy Eng*. 2008;130:011017–011010.
9. Ernst FO, Tricoli A, Pratsinis SE, Steinfeld A. Co-synthesis of H_2 and ZnO by in-situ Zn aerosol formation and hydrolysis. *AIChE J*. 2006;52:3297–3303.
10. Palumbo R, Léde J, Boutin O, Elorza Ricart E, Steinfeld A, Möller S, Weidenkaff A, Fletcher EA, Bielicki J. The production of Zn from ZnO in a high-temperature solar decomposition quench process–I. The scientific framework for the process. *Chem Eng Sci*. 1998;53:2503–2517.
11. L'vov BV, Ugolkov VL, Grekov FF. Kinetics and mechanism of free-surface vaporization of zinc, cadmium and mercury oxides analyzed by the third-law method. *Thermochim Acta*. 2004;411:187–193.
12. Hirschwald W, Stolze F. Zur Kinetik der thermischen Dissoziation von Zinkoxid. *Zeitschrift Physik Chem Neue Folge*. 1972;77: 21–42.
13. Imoto T, Harano Y, Nishi Y. The thermal decomposition of zinc oxide. *Bull Chem Soc Jpn*. 1964;37:1181–1186.
14. Perkins C, Lichty P, Weimer AW. Determination of aerosol kinetics of thermal ZnO dissociation by thermogravimetry. *Chem Eng Sci*. 2007;62:5952–5962.
15. Koumoto K, Yanagida H, Mizuta S. Evaporation of zinc oxide from spinel solid solutions in vacuum. *J Am Ceram Soc*. 1980; 63:17–20.
16. L'vov BV, Ugolkov VL, Grekov FF. Kinetics and mechanism of free-surface vaporization of zinc, cadmium and mercury oxides analyzed by the third-law method. *Thermochim Acta*. 2004;411:187–193.
17. Weidenkaff A, Rellera AW, Wokaun A, Steinfeld A. Thermogravimetric analysis of the ZnO/Zn water splitting cycle. *Thermochim Acta*. 2000;359:69–75.
18. Perkins C, Lichty P, Weimer AW. Thermal ZnO dissociation in a rapid aerosol reactor as part of a solar hydrogen production cycle. *Int J of Hydrogen Energy*. 2008;33:499–510.
19. Möller S, Palumbo R. Solar thermal decomposition kinetics of ZnO in the temperature range 1950–2400 K. *Chem Eng Sci*. 2001;56: 4505–4515.
20. Abanades S, Charvin P, Flamant G. Design and simulation of a solar chemical reactor for the thermal reduction of metal oxides: case study of zinc oxide dissociation. *Chem Eng Sci*. 2007;62:6323–6333.
21. Lédé J, Elorza-Ricart E, Ferrer M. Solar thermal splitting of zinc oxide: a review of some of the rate controlling factors. *J Solar Energy Eng*. 2001;123:91–97.
22. Möller S, Palumbo R. The development of a solar chemical reactor for the direct thermal dissociation of zinc oxide. *J Solar Energy Eng*. 2001;123:83–90.
23. Weidenkaff A, Reller A, Sibieude F, Wokaun A, Steinfeld A. Experimental investigations on the crystallization of zinc by direct irradiation of zinc oxide in a solar furnace. *Chem Mater*. 2000; 12:2175–2181.
24. Schunk LO, Haeberling P, Wepf S, Wuillemin D, Meier A, Steinfeld A. A rotary receiver-reactor for the solar thermal dissociation of zinc oxide. *J Solar Energy Eng*. 2008;130:021009.
25. Haueter P, Seitz T, Steinfeld A. A new high-flux solar furnace for high-temperature thermochemical research. *J Solar Energy Eng*. 1999;121(1):77–80.
26. Tschudi HR, Morian G. Pyrometric Temperature Measurements in Solar Furnaces. *J Solar Energy Eng*. 123(May 2001):164–170.
27. *RoineA Outokumpu HCS Chemistry 5.11*; Outokumpu Research Oy: Pori, Finland, 2002.
28. Suyama Y, Tomokiyo Y, Manabe T, Tanaka E. Shape and Structure of Zinc Oxide Particles Prepared by Vapor-Phase Oxidation of Zinc Vapor. *J Am Ceram Soc*. 1988;71(5):391–395.
29. Chen Z, Shan Z, Cao MS, Lu L, Mao SX. Zinc oxide nanotetrapods. *Nanotechnology*. 2004;15(3):365–369.
30. Müller R, Steinfeld A. H2O-splitting thermochemical cycle based on ZnO/Zn-redox: Quenching the effluents from the ZnO dissociation. *Chem Eng Sci*. 2008;63(1):217–227.
31. Möller S. Entwicklung eines Reaktors zur solarthermischen Herstellung von Zink aus Zinkoxid zur Energiespeicherung mit Hilfe konzentrierter Sonnenstrahlung. PhD Thesis, ETH, Zürich, 2001.
32. Tschudi HR, Schubnell M. Measuring temperatures in the presence of external radiation by flash assisted multiwavelength pyrometry. *Rev Sci Instrum*. 1999;70(6):2719–2727.
33. Secco EA. Decomposition of Zinc Oxide. *Can J Chem*. 1960;38: 596–601.
34. Hirschwald W, Stolze F, Stranski IN. Verdampfung und thermische Dissoziation von Zinkoxid. *Zeitschrift Physik Chem Neue Folge*. 1964;42:96–111.
35. Gray TJ. Sintering of Zinc Oxide. *J Am Ceram Soc*. 1954; 37(11):534–539.
36. Touloukian YS, Ho CY. *Thermophysical properties of matter: the TPRC data series*. New York: Plenum Publishing Corporation; 1972; Vol. 8.
37. Galwey AK, Brown ME. *Thermal Decomposition of Ionic Solids*. Amsterdam: Elsevier; 1999.
38. Whittemore OJ, Varela JA. Initial sintering of ZnO. *Commun Am Ceram Soc*. 1981:C154–C155.
39. Gupta TK, Coble RL. Sintering of ZnO: I Densification and Grain Growth. *J Am Ceram Soc*. 1968;51(9):521–525.
40. Gupta TK, Coble RL. Sintering of ZnO: II Density Decrease and Pore Growth During the Final Stage of the Process. *J Am Ceram Soc*. 1968;51(9):525–528.
41. Pichelin G, Rouanet A. Predictive modeling of high-temperature chemical system vaporization under atmospheric pressure. *Chem Eng Sci*. 1991;46(7):1635–1649.
42. Millar J, Palumbo RD, Rouanet A, Pichelin G. The production of Zn from ZnO in a two-step solar process utilizing FeO and Fe3O4. *Energy*. 22(2–3):301–309, 1997.
43. Palumbo R, Rouanet A, Pichelin G. The solar thermal decomposition of TiO2 at temperatures above 2200 K and its use in the production of Zn from ZnO. *Energy*. 1995;20(9):857–868.
44. L'vov BV. Interpretation of atomization mechanisms in electrothermal atomic absorption spectrometry by analysis of the absolute rates of the processes. *Spectrochim Acta Part B*. 1997;52(1):1–23.
45. Gunze M, Hirschwald W, Thull E. Der Einfluss einer intensiven Sauerstoffbehandlung auf die thermische, chemische und photochemische Stabilität von Zinkoxid. *Zeitschrift Physik Chem Neue Folge*. 1976;100:201–216.
46. Xu G-f, Lloyd IK, Olorunyolemi YCaT, Wilson OC. Microwave sintering of ZnO at ultra high heating rates. *J Mater Res*. 2001; 16(10):2850–2858.
47. Birnboim A, Gershon D, Calame J, Birman A, Carmel Y, Rodgers J, Levush B, Bykov YV, Eremeev AG, Holoptsev VV, Semenov VE, Dadon D, Martin PL, Rosen M, Hutcheon R. Comparative Study of Microwave Sintering of Zinc Oxide at 2.45, 30, and 83 GHz. *J Am Ceram Soc*. 1998;81(6):1493–1501.
48. Cussler EL.*Diffusion*.London:Cambridge University Press; 1984.

49. Kendoush AA. Theory of convective heat and mass transfer to fluids flowing normal to a plane. *Int Commun Heat Mass Transfer*. 1996;23(2):249–262.
50. L'vov BV. Recent advances in absolute analysis by graphite furnace atomicabsorption spectrometry. *Spectrochim Acta Part B: Atom Spectrosc*. 1990;45(7):633–655.
51. Fuller EN, Schettler PD, Giddings JC. A new method for prediction of binary gas phase diffusion coefficients. *Ind Eng Chem.* 1966;58(5):19–27.
52. Schunk LO, Lipínski W, Steinfeld A. Ablative heat transfer in a shrinking packed-bed of ZnO undergoing solar thermal dissociation. *AIChE J*, in press.

Manuscript received Jan. 15, 2008, and revision received Nov. 1, 2008.